Smart Structures and Systems, *Vol. 35, No. 4 (2025) 209-219*
https://doi.org/10.12989/sss.2025.35.4.209

Carbon nanotube cementitious composites model with pore conductivity for ship-bridge collision monitoring

Jian Guo*[1], Yuhao Cui [2a] and Shan Hu [3b]

[1] *State Key Laboratory of Bridge Intelligent and Green Construction, Southwest Jiaotong University, Chengdu, Sichuan 610000, China*
[2] *School of Civil Engineering, Southwest Jiaotong University, Chengdu, Sichuan 610000, China*
[3] *Institute of Bridge Engineering, Zhejiang University of Technology, Hangzhou, Zhejiang 310012, China*

(*Received December 24, 2024, Revised April 18, 2025, Accepted May 20, 2025*)

Abstract. This study introduces a novel carbon nanotube (CNT) cementitious composite sensor developed using pore conductivity theory to address durability and structural compatibility requirements for monitoring ship-bridge collisions in marine environments. The sensor employs a dual-channel sensing mechanism by integrating CNT networks with conductive pathways formed by electrolyte solutions within cement pores. Experimental results demonstrate high sensing accuracy across sensors with varying slenderness ratios, achieving axial and lateral errors under 8%. Notably, sensors with a 1:4 slenderness ratio exhibit significantly enhanced resistance change rates under axial loading, up to 281% within a 10 kN lateral load range. Impact tests further confirm strong correlation between electrical signals and strain gauge measurements when collision speeds range between 1-2 m/s, validating real-time collision damage monitoring capabilities. This research establishes design principles for pore conductivity-based CNT cement sensors while providing theoretical foundations for smart concrete applications in ship-bridge collision monitoring.

Keywords: carbon nanotubes; cementitious composite; impact load; pore conductivity; sensing model

1. Introduction

In marine environments, bridges are subject to loads from road vehicles, and their piers may also endure impacts from ship collisions, as depicted in Fig. 1. Under such circumstances, the reaction forces acting on the bridge supports, the impact loads resulting from ship collisions, and the subsequent internal damage are mainly confined within the structure. Furthermore, the support forces arising from ship-bridge collisions undergo rapid fluctuations. Traditional sensors struggle to effectively monitor these conditions. Therefore, sensors used for monitoring ship-bridge collisions must exhibit exceptional compatibility with concrete structures and possess the ability to detect both high-frequency static and dynamic loads (Wen and Chung 2001, Fantuzzi *et al*. 2017).

Carbon nanotubes (CNTs) were officially recognized and named in 1991 (Iijima 1991). Extensive research has demonstrated the exceptional mechanical properties (Mohammadimehr and Alimirzaei 2017, Rostami *et al*. 2020) and excellent electrical conductivity exhibited by CNTs (Park *et al*. 2021, Lee *et al*. 2022, Zidour *et al*. 2022). When incorporated into carbon nanotube cementitious composites, CNTs not only enhance the strength of the composites but also confer piezoresistive characteristics and self-inductive functionality upon the cementitious material (Li *et al*. 2007, Khater and Abd El Gawaad 2015). Consequently, these highly compatible, durable, and cost-effective composites have emerged as promising candidates for sensor applications in the field of civil engineering materials. They effectively mitigate several inherent limitations of conventional sensors, thus ensuring their extensive applicability, particularly in the realm of construction materials (Kumar *et al*. 2012, Danoglidis *et al*. 2016). CNT composite sensors are expected to solve the problem of monitoring ship-bridge collisions. Currently, they have attracted a great deal of interest from researchers (Deng and Zheng 2008, Konsta-Gdoutos *et al*. 2010).

It is crucial to thoroughly comprehend the interplay between CNTs and the properties of the composite material when applying CNT cementitious composite for ship-bridge collision monitoring. Research indicates that incorporating a small amount of CNTs, especially within a water-cement ratio range of 0.45 to 0.60, significantly enhances the compressive strength of cement paste/mortar (Han *et al*. 2012). Meanwhile, CNT composites exhibit exceptional linear piezoresistive properties under static loading conditions, making them ideal for stress monitoring applications (Saafi 2009, Parvaneh and Khiabani 2019). Konsta-Gdoutos and Aza (2014) examined the self-sensing properties of well-dispersed CNTs and carbon nanofiber-reinforced cement-based composites, discovering that nanocomposites containing 0.1wt% CNTs exhibit enhanced electrical properties, and the addition of both CNTs and carbon nanofibers further amplifies changes in resistance. Suchorzewski *et al*. (2020) noted that incorporating minute

*Corresponding author, Ph.D., Professor,
E-mail: Guoj@swjtu.edu.cn
[a] Ph.D. candidate, E-mail: cuiyuhao@my.swjtu.edu.cn
[b] Master's student, E-mail: hushan0204@163.com

ISSN: 1738-1584 (Print), 1738-1991 (Online)

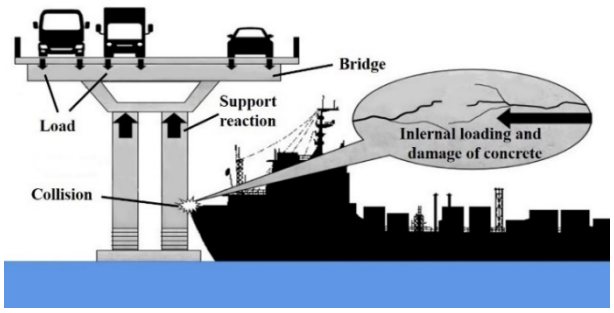

Fig. 1 Engineering background

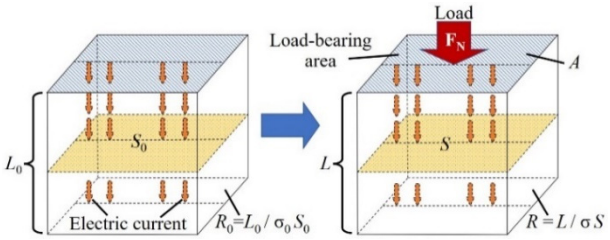

Fig. 2 Relationship between resistance and load

amounts of multi-walled CNTs improves the stress detection capabilities of sensors and enables microcrack monitoring. Micromechanical models reveal that the superior piezoresistive characteristics of CNT composite sensors stem from the formation of CNT networks, anisotropic conductivity, and unique waveform properties (Deng and Zheng 2008, Takeda *et al*. 2011). Theodosiou and Saravanos (2010) utilized atomic models and numerical simulations to uncover the primary mechanisms governing the strain sensitivity of composites, including CNT resistance and tunneling effects. Yasuoka *et al*. (2010) employed circuit simulators to model percolation networks and investigate the strain sensitivity of CNT-based composites, discovering a highly nonlinear behavior in the simulated piezoresistive coefficient. Furthermore, Garcia-Macias *et al*. (2017) introduced a prediction method grounded in micromechanics, which considers strain-induced variations in volume fraction to forecast the piezoresistive effects of CNT-cementitious composites, validated under uniaxial compression conditions. Currently, much research focuses on the resistive characteristics of CNT composite sensors under linear static or cyclic pressure (Ubertini *et al*. 2014, Sasmal *et al*. 2017).

Previous studies have examined the piezoresistive properties of CNT cementitious composite sensors and developed micromechanical models, yet challenges persist when applying these sensors in marine environments. The internal pores in CNT cementitious composites are vulnerable to erosion by solutions, which affects their piezoresistive performance and the accuracy of dynamic monitoring. Additionally, systematic investigations into the piezoresistive variation mechanisms of the sensors under high-strain dynamic loading conditions during ship-bridge collisions remain insufficient. To resolve these issues, a novel electrical response calculation model was developed that accounts for pore conductivity principles. The model's feasibility and effectiveness were demonstrated through uniaxial compression tests and impact loading experiments, providing theoretical support and technical pathways for intelligent monitoring of ship-bridge collision events.

2. The establishment of the sensing model

In marine environments characterized by high humidity, large concrete structures, including sea bridges, are commonly encountered. The conductivity of the internal pore solution significantly impacts the sensing characteristics of CNT cementitious composites when incorporated within such structures (Meira *et al*. 2010). Therefore, it is crucial to account for the influence of pore conductivity when developing models to characterize the sensing behavior of these composites.

2.1 The relationship between resistance and load

The response of the CNT cementitious composite is characterized by the variation in resistance, as illustrated in Fig. 2. Specifically, in the context of uniaxial compression, the rate of change in resistance for the test specimen can be calculated using Eq. (1).

$$\mathrm{FCR}=\frac{\Delta R}{R_0}=\frac{\sigma_0 L S_0}{\sigma L_0 S}-1 \tag{1}$$

Where FCR is the rate of resistance change; ΔR is the resistance change value of the sensor; R_0 is the initial resistance of the sensor; σ_0 and σ are the conductivity of the sensor before and after loading, respectively; L is the length of the specimen; S is the cross-sectional area of the specimen; L_0 and S_0 are the length and cross-sectional area of the specimen before loading.

Given that conductivity is the reciprocal of resistivity, it becomes possible to deduce Eq. (2) by incorporating the relationship between strain and load.

$$\begin{cases}\Delta R/R_0=\dfrac{\sigma_0(1+\varepsilon_0)}{\sigma(1-\nu\varepsilon_0)^2}-1\\ \varepsilon_0=\dfrac{F_N}{EA}\end{cases} \tag{2}$$

Where ε_0 is the axial strain of the specimen; ν is the Poisson's ratio of the specimen; F_N is the compressive load; E is the elastic modulus of the sensor and A is the load-bearing area of the sensor.

2.2 Conductivity model

Obtaining a model for the conductivity of composites is of utmost importance due to its close relationship with strain. Considering the excellent one-dimensional conduction properties of CNTs, it is assumed that the initially irregularly curved CNTs become straight and uniformly distributed within the cement matrix. Fig. 3 presents a schematic diagram illustrating the equivalent length of a CNT, where L_{el} represents the length of the CNT

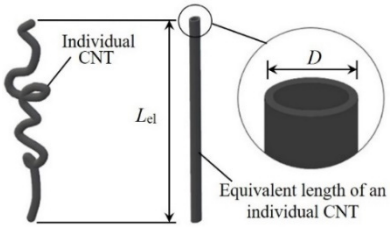

Fig. 3 Schematic diagram of the equivalent length of a CNT

and D denotes the tube diameter (Deng and Zheng 2008).

Fig. 4 illustrates the assumed dual conductive modes present in CNT cementitious composites: pore solution and CNTs within the cementitious material. When the sensor is subjected to loading, a series of internal changes take place, including a reduction in porosity and an augmentation in contact points.

In order to establish a sensor conductivity model that takes into account the conduction of pore solution, Eq. (3) can be derived based on the aforementioned dual conduction mode in CNT cementitious composites.

$$\sigma = (1-\varphi)\sigma_{\text{cm}} + \varphi\sigma_w \tag{3}$$

where φ is the porosity of the composite, σ_{cm} is the conductivity of the CNTs composite cement matrix and σ_{w} is the conductivity of the cement matrix pore solution. Eq. (4), which represents the relationship between the resistance change rate and the dual conductive pathways in the cement matrix established in this study, can be obtained by substituting Eq. (3) into Eq. (2).

$$\frac{\Delta R}{R_0} = \frac{\sigma_w\varphi_0 + (1-\varphi_0)\sigma_{\text{cm0}}}{\sigma_w\varphi_1 + (1-\varphi_1)\sigma_{\text{cm1}}}\frac{1+\varepsilon_0}{(1-\nu\varepsilon_0)^2} - 1 \tag{4}$$

where φ_0 and φ_1 are the porosity before and after loading, respectively; σ_{cm0} and σ_{cm1} are the conductivity of the CNTs composite cement matrix before and after loading, respectively.

The calculation of σ_{cm} plays a critical role in determining the rate of resistance change in the composite. It is assumed that the CNTs within the cementitious composite are straight and uniformly distributed. The determination of σ_{cm} can be achieved using the micromechanical method proposed by Mori and Tanaka (1973), as described in Eqs. (5)-(7).

$$\sigma_{\text{cm}} = \sigma_m\left\{1 + \frac{fT}{1-f[1-T/(\sigma_c/\sigma_m - 1)]}\right\} \tag{5}$$

$$T = \frac{\sigma_c/\sigma_m - 1}{3}\left[\frac{2}{1+(\sigma_c/\sigma_m - 1)S_{11}} + \frac{1}{1+(\sigma_c/\sigma_m - 1)S_{33}}\right] \tag{6}$$

$$S_{11} = \begin{cases} \dfrac{\eta}{2(\eta^2-1)^{3/2}}\left[\eta(\eta^2-1)^{1/2} - \cos h^{-1}\eta\right] \eta > 1 \\ \dfrac{\eta}{2(1-\eta^2)^{3/2}}\left[\cos h^{-1}\eta - \eta(1-\eta^2)^{1/2}\right] \eta < 1 \end{cases} \tag{7}$$

where η is the length-to-diameter ratio of CNTs, $\eta = L_{\text{el}}/D$; L_{el} is the equivalent length of CNTs, D is the diameter of CNTs, σ_{c}, σ_{m} are the conductivity of CNTs and tunnel penetration conductivity, $S_{33} = 1 - 2S_{11}$, f is the volume fraction of CNTs, this is a parameter that can be designed and predetermined. According to the study by Simmons and Unterkofler (1963), on the tunneling effect, tunneling conductivity σ_{m} can be obtained by Eq. (8).

$$\sigma_m = \frac{e^2(2m\lambda)^{1/2}}{h^2} exp\left[-\frac{4\pi d_a}{h}(2m\lambda)^{1/2}\right] \tag{8}$$

where λ is the barrier height, m is the mass of the electron, e is the charge carried by the electron, h is Planck's constant, d_{a} is the tunneling spacing of the electron transition, the values of which are solved according to Eq. (9) based on the theory of Deng and Zheng (2008).

$$d_a = \begin{cases} d_c \\ d_c\left(\dfrac{f_c}{f}\right)^{1/3} \end{cases} \tag{9}$$

where f_{c} is the seepage threshold of CNTs, d_{c} is the average spacing of CNTs when the seepage threshold is reached, and here $d_{\text{c}} = 0.5$ nm (Wen and Chung 2001, Meira *et al.* 2010, Xu *et al.* 2010). Deng and Zheng (2008) also proposed Eqs. (10)-(11) for determining the percolation threshold.

$$f_c = \frac{9H(1-H)}{2+15H-9H^2} \tag{10}$$

$$H = \frac{1}{\eta^2-1}\left[\frac{\eta}{\sqrt{\eta^2-1}} ln\left(\eta + \sqrt{\eta^2-1}\right) - 1\right] \tag{11}$$

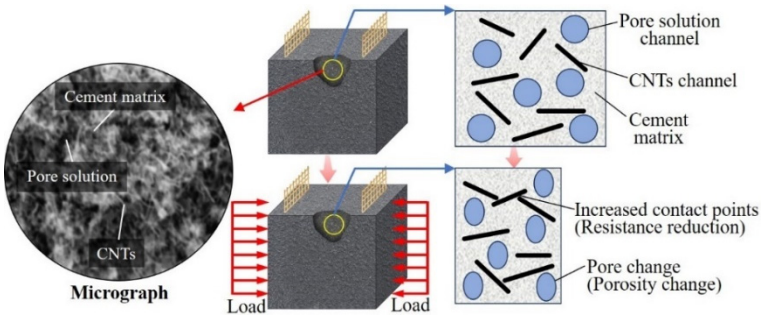

Fig. 4 Two conductive channels exist in the cement matrix

As the conductivity of the pore solution remains constant throughout loading, the variation in resistance of the sensor can be determined by establishing the porosity change pattern. A physical model of a two-phase composite is employed to assess the porosity change. The cement-containing pores are simplified using an isotropic elastic hollow sphere model (Christensen and Lo 1979, Duan *et al.* 2006), where the pores are located within the interior and the cement matrix surrounds them. Under this assumption, the relationship between porosity and volumetric strain is described by Eqs. (12)-(13).

$$\varphi_1 = \frac{\varphi_0}{1-\theta} \cdot \Theta \tag{12}$$

$$\Theta = \left[1 - \frac{\left(1-\sqrt[3]{1-\theta}\right)(4\mu_m + 3k_m)}{4\mu_m + 3\varphi_0 k_m}\right]^3 \tag{13}$$

wherer θ is the usual spherical polar coordinates, μ_m and k_m are the shear modulus and volume modulus of CNT cementitious composites, respectively.

3. Experiment

This section presents experimental designs aimed at validating the accuracy of the model and examining the response characteristics of the composites under impact loading. Cementitious composite sensors with varying concentrations of aminated multi-walled CNTs were fabricated. The resistive change rate was evaluated by subjecting the sensors, in both cubic and prismatic shapes, to uniaxial compression and impact tests.

3.1 Aminated multi-walled CNTs

It has been demonstrated that aminated multi-walled carbon nanotubes (AMCNTs) exhibit improved dispersibility and reduced agglomeration compared to regular CNTs. Consequently, they can be uniformly dispersed within the gel material, providing enhanced mechanical and electrical properties for CNT cementitious composites (Sahoo *et al.* 2010, Zhang *et al.* 2011). Table 1 presents the technical parameters of various CNT types. Notably, the high aspect ratio and excellent conductivity of AMCNTs contribute to the superior electrical conductivity of the composite materials, thereby ensuring the high reliability of the experimental results.

Table 1 Technical parameters of different types of CNTs

Type	Length-to-diameter ratio	Density (g/cm^3)	Resistivity (μΩ·m)
Ordinary CNTs	200-750	0.07	800
AMCNTs	750-2000	0.15	1800

Table 2 Mixing ratio

Code	Water (kg/m^3)	Portland cement (kg/m^3)	W/C (kg/m^3)	Sand (kg/m^3)	CNTs (%)
1	352.94	784.31	0.45	862.75	0.05
2	352.94	784.31	0.45	862.75	0.10
3	352.94	784.31	0.45	862.75	0.25

AMCNTs were employed for the fabrication of CNT cementitious composite sensors. The preparation of AMCNTs involved subjecting multi-walled carbon nanotubes to a free radical reaction, followed by reduction using an Al-$NiCl_2$·$6H_{20}$-THF system. Table 1 provides technical parameters for different CNT types. The purity of the AMCNTs utilized in the experiments exceeded 98%.

3.2 Mixing ratio and specimen preparation

The experimental procedures adhered to the national standard (GB175-2007) for Portland P.O 42.5 cement and the ISO standard (ISO679:1989 and EN196-1) for sand, which were utilized in the production of the cement matrix for the composite. To ensure the construction of a conductive network in the cement matrix while keeping costs low, the maximum content of AMCNTs was set at 0.25%, surpassing the permeation threshold. The specimens were prepared with AMCNT contents of 0.05%, 0.10%, and 0.25% by weight of cement to assess the performance of the composite under static and impact loads at various CNT concentrations. It should be noted that the dispersion of CNTs is influenced by the water-cement ratio (W/C). A higher W/C ratio can lead to CNT aggregation and increased porosity (Kim *et al.* 2017). Therefore, a W/C ratio of 0.45 was chosen to achieve optimal electrical conductivity (Han *et al.* 2012, Kim *et al.* 2014). The mixing ratio is presented in Table 2.

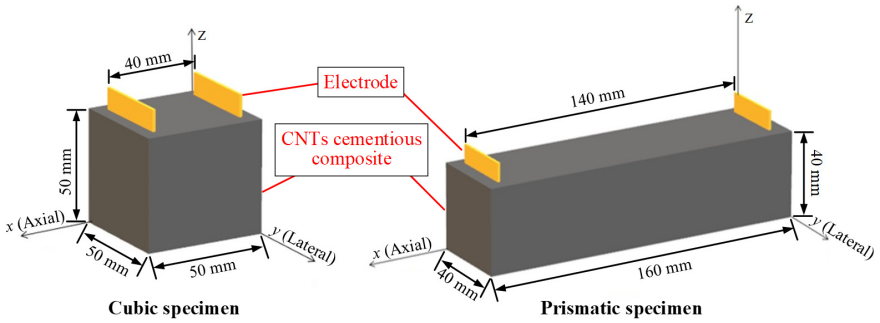

Fig. 5 The samples diagram

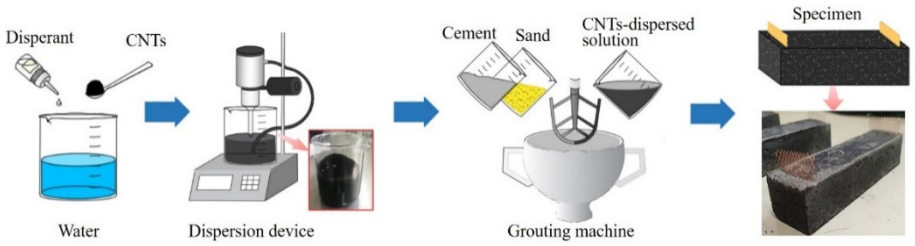

Fig. 6 Preparation procedure for CNT cementitious sensors

Eq. (2) highlights the close relationship between the resistance variation and the shape of the composite specimen (ε_0, A). To investigate this relationship and validate the accuracy of the model, two types of sensors, namely cubic and prismatic, were designed, as depicted in Fig. 5. The cubic group has dimensions of 50 × 50 × 50 mm with an electrode spacing of 40 mm, while the prismatic group has dimensions of 40 × 40 × 160 mm with an electrode spacing of 140 mm. As the electrodes are in sheet form, the direction perpendicular to the electrode plane is defined as the axial direction, while the direction parallel to the electrode plane is defined as the transverse direction.

An aqueous dispersion solution and an ultrasonic crusher were utilized to achieve uniform dispersion of AMCNTs (Xie *et al*. 2005). Initially, the dispersion solution was dissolved in water, followed by the addition of CNTs and stirring. Ultrasonic dispersion was then initiated, and centrifugation was performed to obtain the final CNT dispersion. Subsequently, the dispersed CNT solution was poured into a stirring pot, where silicate cement was added. The stirring pot was operated for 2 minutes, after which standard sand was introduced and stirred for 4 minutes. The stirring equipment was then turned off, allowing the mixture to settle for 2 minutes before restarting the equipment for an additional 4 minutes. Finally, the resulting mixture was poured into a mold and allowed to solidify, forming the sample. For impact load testing, composite prismatic specimens containing 0.05% and 0.10% CNT content were fabricated using the same method. The specific preparation process and production steps of the CNT cementitious sensor are illustrated in Fig. 6.

3.3 Test methods

3.3.1 Uniaxial compression test

Uniaxial compression tests were conducted on both cubic and prismatic specimens. The accuracy of the model was assessed by evaluating the electrical conductivity variations in both axial and lateral directions of specimens under varying compressive loads.

The uniaxial compression tests on the CNT cementitious sensors were performed using the WDW-50 Microcomputer-controlled Electronic Universal Testing Machine. The tests were conducted in both the axial and lateral directions. The testing machine employed a loading rate of 100 N/s, and the data acquisition frequency was set at 5 Hz. The electrical signal of the sensor was collected using the VC8246B multimeter at a frequency of 2 Hz. Both signals were sampled to 1Hz for synchronized analysis. The test specimens had dimensions of 50 × 50 × 50 mm. To eliminate resistance drift caused by sensor polarization, all sensors were energized for 6000 s prior to the test (Cao and Chung 2004). To ensure the representativeness and reliability of the results, two sets of data were extracted and averaged after multiple tests. Fig. 7 illustrates the uniaxial compression test conducted on the CNT composite sensor specimen.

3.3.2 Impact load test

In the impact load testing, impact forces were induced

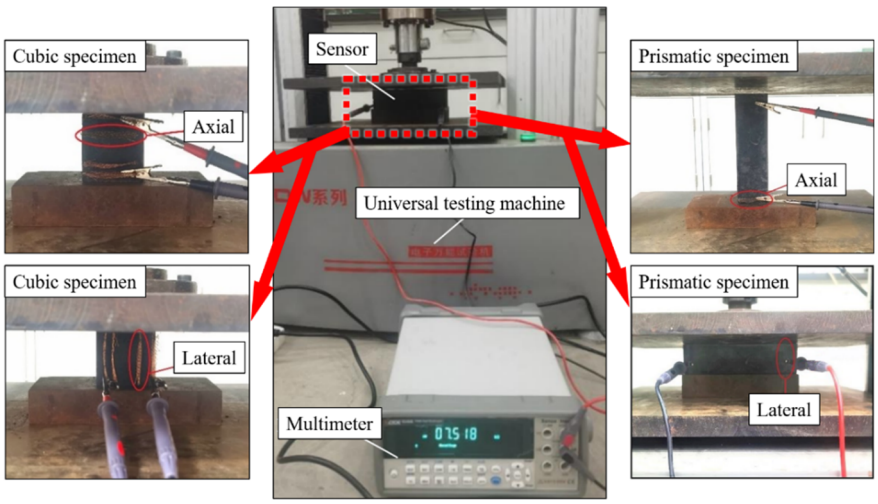

Fig. 7 the uniaxial compression test of the CNT composite sensor specimen

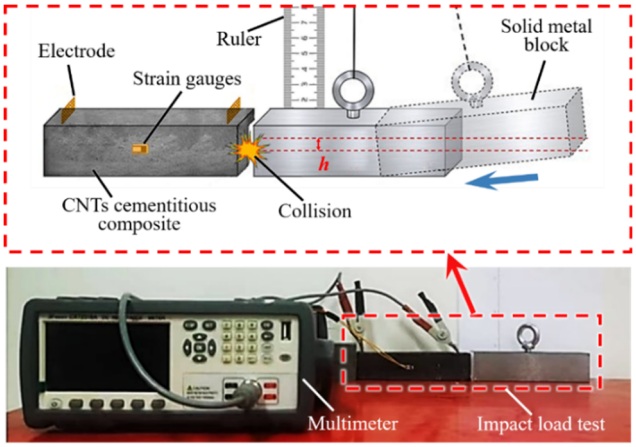

Fig. 8 The method of applying impact load

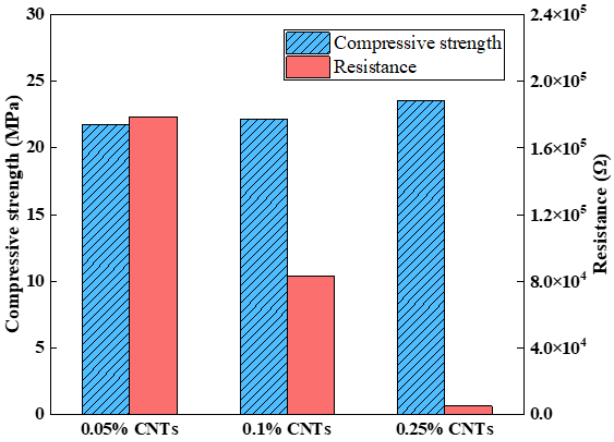

Fig. 9 The compressive strength and resistance of different samples

through the free-fall motion of a pendulum. A solid metal block, weighing 2 kilograms and featuring a cross-sectional area of 16 square centimeters, was connected to one end of a rope, while the opposing end was anchored to a metal ruler. The prismatic specimen was securely fastened to the base, ensuring alignment of its right side with the rope. As the metal block swung to its lowest position, its cross-section precisely coincided with that of the prismatic specimen. To achieve diverse magnitudes of impact loads, the release height of the metal block was varied, resulting in velocities of 0.5 meters per second, 1.0 meter per second, and 2.0 meters per second. Electrical measurements were performed utilizing a Xinyang CXT2516A-DC resistance tester. Given the extremely brief duration of the shock loads, the system was configured to acquire shock load data at a sampling rate of 20 Hertz, enabling the detailed capture of information throughout the shock process (Simmons and Unterkofler 1963, Mori and Tanaka 1973, Wen and Chung 2001, Fantuzzi *et al*. 2017). Strain gauges were bonded to the surface of the specimen to quantify the strain variations within the composite material under impact loading conditions. The precise methodology for applying the impact load is depicted in Fig. 8.

4. Results and discussion

4.1 Compressive strength and resistance

The compressive strength of the sensor is crucial for ensuring the durability and compatibility of CNT cementitious composites, while the electrical resistance reflects the electrical conductivity of the composites. Fig. 9 illustrates the compressive strength and electrical resistance of prisms with varying CNT contents. From the figure, it can be observed that the compressive strength of the specimens increases with higher CNT content, although the change is not significant. The compressive strength of all prismatic specimens remained at approximately 23 MPa, slightly surpassing that of ordinary cementitious prisms. This characteristic is favorable for the sensing capabilities of CNT cementitious composites. Excessive strength of the sensors hinders the deformation of the composites and impacts their electrical properties, while insufficient strength results in poor compatibility and durability of the composites within the structure.

In contrast to the pattern observed in compressive strength, it is evident that the resistance values of samples with varying CNT contents exhibit significant differences, consistent with findings reported by Konsta-Gdoutos and Aza (2014). Specifically, the resistance value of the specimen with 0.1% CNT content is approximately half that of the 0.05% group, while the resistance value of the specimen with 0.25% CNT content is only 6% of that in the 0.1% group. This discrepancy can be attributed to the percolation effect (Xie *et al*. 2005, Deng and Zheng 2008), with the percolation threshold for CNT cementitious composites estimated to be around 0.2%.

Once the CNT content reaches this threshold, CNTs establish a complete conductive network within the composites, resulting in a significant decrease in the electrical resistance of the material. Beyond this threshold, further increases in CNT content do not lead to significant reductions in electrical resistance. These results validate the potential of CNT cementitious composites as sensors for structural health monitoring. Notably, the selection of the CNT content is a crucial parameter for the composites.

4.2 Analysis of test results of the cube group

The response of the cubic sensor to loads in different directions should theoretically exhibit consistency, as the CNTs are uniformly dispersed in the cement matrix, as stated in Eq. (6). Fig. 10 presents the variation pattern of FCR with load and its corresponding fitting curve for the cubic sensor subjected to axial and lateral loading. As depicted in the figure, the resistance value decreases with increasing load during both axial and lateral loading tests. The FCR of the specimen is highly sensitive to applied stress changes, establishing it as a viable piezoresistive sensor (Konsta-Gdoutos and Aza 2014). Initially, during the early stages of loading, the resistive change rate of the sensor in both directions is very similar, and the trends of the two fitted curves closely align. This consistency with theoretical analysis results suggests the sensor's efficacy in

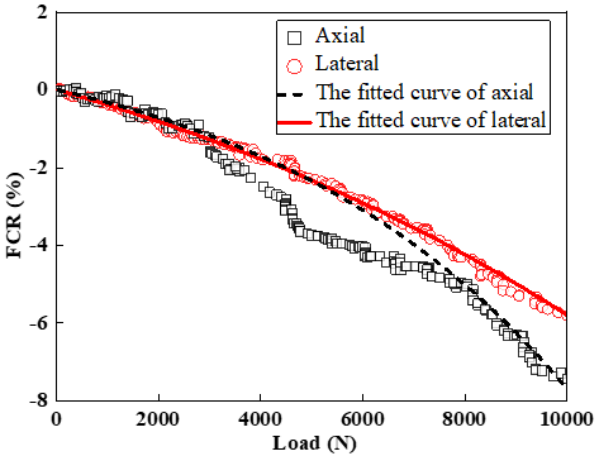

Fig. 10 Variation of FCR with load for cubic sensors

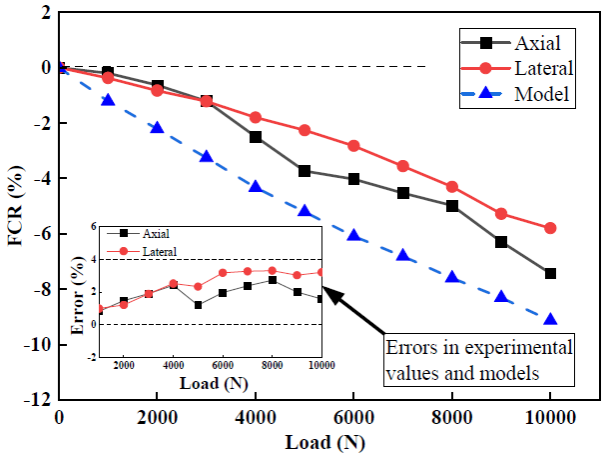

Fig. 11 Comparison of experimental and model-calculated values for the rate of resistance change of cubic sensors

load monitoring.

However, in the middle and later stages of loading, the resistance change rate under axial loading slightly exceeds that under transverse loading. This disparity can be attributed to the electrodes buried within the sensor, which act as a deformation barrier as deformation increases in the middle and later stages of transverse loading. Consequently, optimizing parameters such as the material, position, and shape of the electrodes becomes crucial to minimize their influence on the sensor's test results in practical applications.

Fig. 11 illustrates the variation of FCR of the cubic sensor calculated from the model. Observing the figure, it is evident that the absolute value of the resistance change rate calculated by the model slightly exceeds the experimental values for both axial and lateral loads. This discrepancy arises from the limitation on sensor deformation during the compression test, resulting from friction on the compression surface. Consequently, the actual resistance rate of change is lower than the calculated value. Since CNT cementitious composite sensors are typically integrated into concrete structures, researchers must consider the effect of the concrete contact surface on the sensing performance in practical applications.

To assess the accuracy of the model, a comparative analysis was conducted between the experimental and model-calculated values to determine the error. The error is calculated as the difference between the experimental FCR and the FCR calculated by the model. It was observed that the model's error remains below 4% for both axial and lateral directions, representing a low level of discrepancy. This indicates the successful computation of the model for the cubic sensor.

4.3 Analysis of test results of the prism group

Fig. 12 displays the variation pattern of FCR with load and its corresponding fitting curve for prismatic sensors subjected to axial and lateral loading. Examining the figure, it is evident that the prismatic sensor exhibits a favorable conductive response to the applied load. However, the response to the load differs between the two loading directions. Under transverse loading, the resistance change at the beginning of the loading is slower compared to the end, similar to the trend observed in the cube group test. Conversely, the prismatic group demonstrates a significantly higher rate of resistance change under axial loading, unlike the cubic sensor. This variation can reach a maximum of 281% within the 10 kN load range for transverse loading, indicating that an increase in the slenderness ratio enhances the sensitivity of the sensor. Consequently, prismatic specimens prove more suitable for the fabrication of CNT cementitious composite sensors.

Fig. 13 depicts the variation pattern of FCR of prismatic CNT cementitious composites calculated from the model. The figure illustrates that the model-calculated prismatic sensors exhibit different FCR responses to load under two distinct loading directions. The primary reason for this discrepancy lies in the change in force area of the prismatic sensor group when the load direction is altered. Consequently, the sensors experience varying deformations under the same load, leading to macroscopic differences in the rates of resistance change.

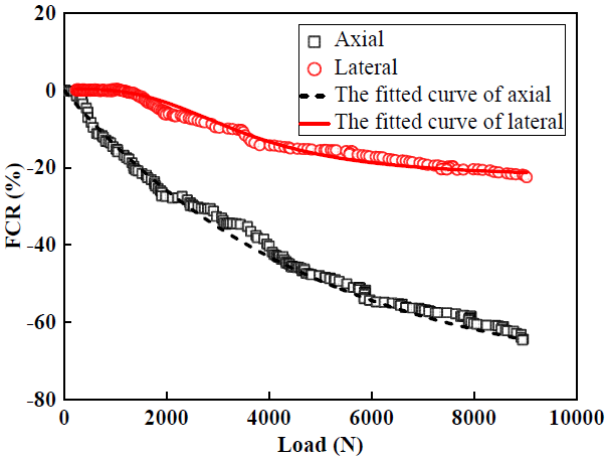

Fig. 12 Variation of FCR with load for prismatic sensors

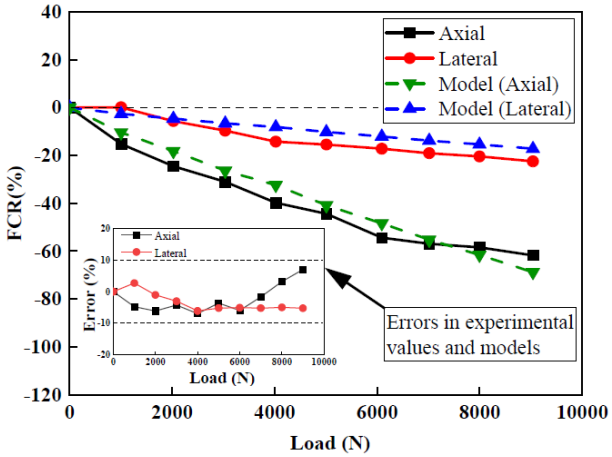

Fig. 13 Comparison of experimental and model-calculated values for the rate of resistance change of prismatic sensors

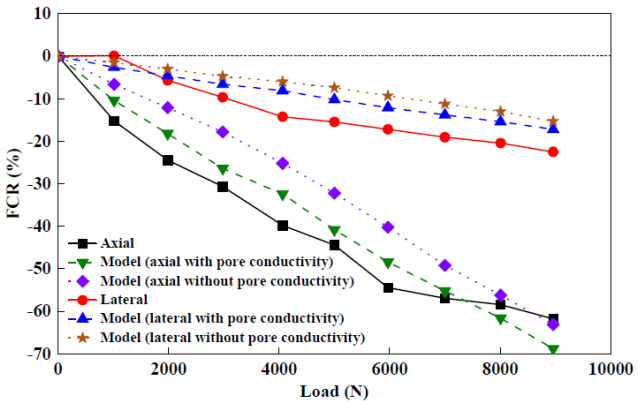

Fig. 14 Comparison of experimental and calculated values of FCR without considering void conductivity

By calculating the error between the experimental and model-calculated values, it is observed that the model's error remains mostly below 8% for both axial and transverse directions, indicating good accuracy and affirming the model's applicability. Notably, the calculated values from the model are generally lower than the experimental results under different loading directions, which contrasts with the findings of the cubic group. This discrepancy arises due to the relatively larger size and presence of internal defects in the prismatic specimens compared to the cubic specimens. These factors result in relatively larger deformations, counteracting the limitations imposed by friction on specimen deformation and causing the experimental values to slightly surpass the model's calculated values. This observation also inspires researchers to consider parameter optimization and selection in sensor design.

Additionally, the rate of resistance change for the prismatic group is calculated without accounting for pore conductivity, as per Eq. (14) modified from Eq. (4).

$$\frac{\Delta R}{R} = \frac{(1-\varphi_0)\sigma_{\mathrm{cm0}}}{(1-\varphi_1)\sigma_{\mathrm{cm1}}} \frac{1+\varepsilon_0}{(1-\nu\varepsilon_0)^2} - 1 \tag{14}$$

The variation in resistance change rate of the model for the prismatic group is presented in Fig. 14. It is noteworthy that the absolute value of the resistance change rate remains relatively small when pore conductivity is not considered. However, under lateral loading, the disparity between considering and not considering pore conductivity is more pronounced compared to axial loading. This finding provides evidence supporting the rationale for considering the influence of pore conductivity on the properties of CNT cementitious composites.

Meanwhile, it can be observed that the effect of pores on the rate of resistance change in CNT cementitious composites diminishes with increasing load. This trend arises from the internal densification of the material as the load increases, resulting in a decrease in the impact of pore conductivity. Nevertheless, it should be noted that the influence of pore conductivity remains non-negligible, even as the material becomes denser under load.

4.4 Analysis of test results under impact load

Fig. 15 illustrates the strain and FCR responses of composite sensors with varying CNT contents under impact loading. Observing the figure, it is evident that the resistance of the sensors exhibits a sudden drop immediately after impact at an impact velocity of 0.5 m/s, followed by a rapid recovery to an approximate initial value. This behavior stems from the relatively small impact load, which induces elastic deformation in the composite material during the impact event and increases the density of conductive pathways within the material. Consequently, the resistance of composite material decreases.

The composite sensor's resistance also undergoes a sharp and more substantial decrease upon impact at an impact velocity of 1.0 m/s, resembling the pattern observed in the composite resistance decreasing with increasing static load. However, in this case, the composite resistance does not return to its approximate initial value after impact but instead displays a more pronounced and permanent increase. This phenomenon is postulated to result from a combination of microscopic factors, including plastic deformation within the composite under large impact loads, and the creation of numerous microcracks that hinder the connectivity of CNT conductive paths within the material, leading to a macroscopic increase in composite resistance.

These speculations find support in the results obtained at an impact velocity of 2.0 m/s. As the impact load increases, the sensors experience greater deformation and develop more internal defects, both of which manifest as changes in resistance. Furthermore, sensors with different CNT contents exhibit similar response patterns to impact loading, demonstrating consistent trends in FCR and strain. This observation suggests that the electrical response of CNT cementitious composites following impact loading is predictable and regular.

Moreover, the electrical response of the sensor maintains good correspondence with the measured values of strain gauges after impact loading. Additionally, as a cement-based sensor, it can be conveniently installed as part

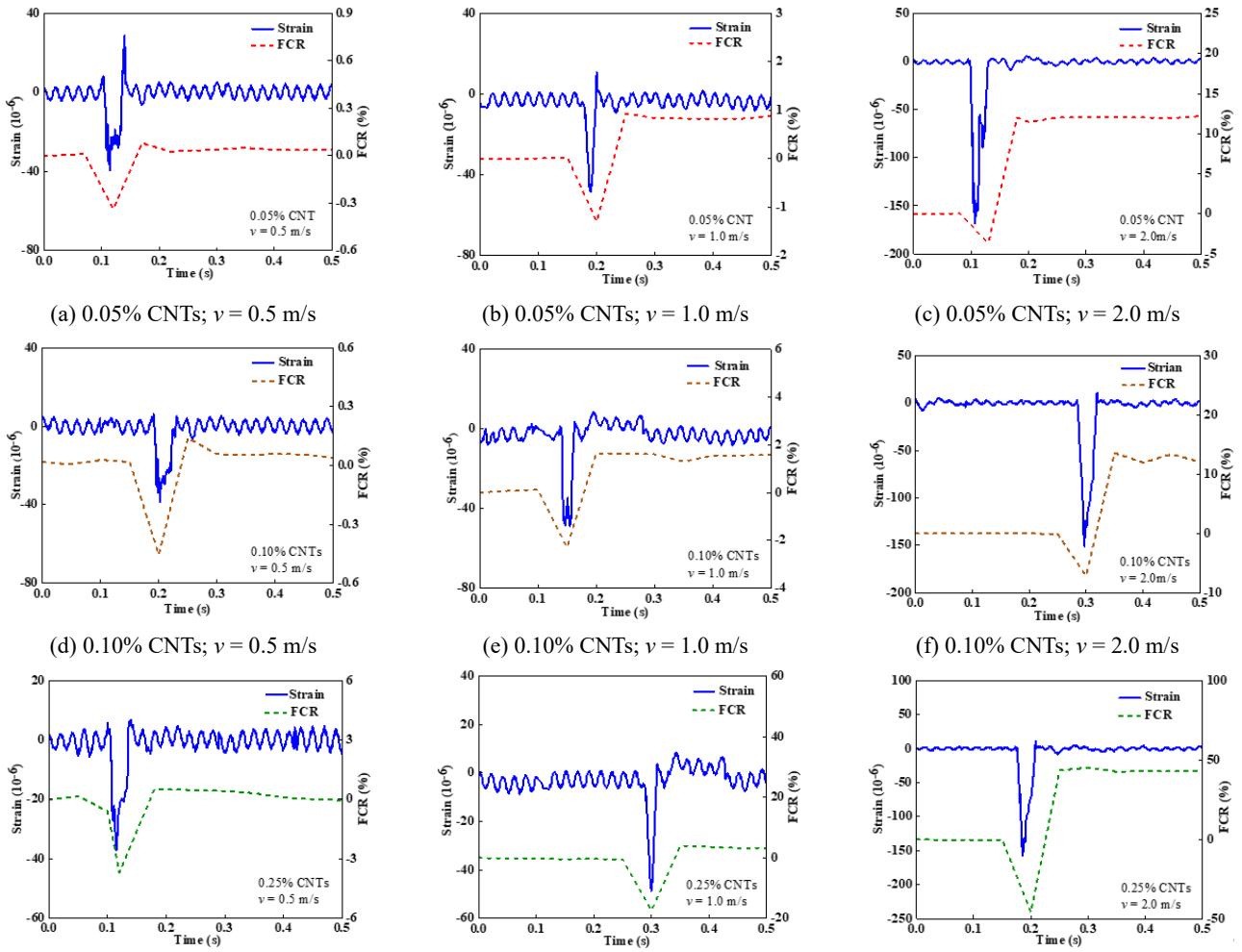

(a) 0.05% CNTs; v = 0.5 m/s (b) 0.05% CNTs; v = 1.0 m/s (c) 0.05% CNTs; v = 2.0 m/s

(d) 0.10% CNTs; v = 0.5 m/s (e) 0.10% CNTs; v = 1.0 m/s (f) 0.10% CNTs; v = 2.0 m/s

(g) 0.25% CNTs; v = 0.5 m/s (h) 0.25% CNTs; v = 1.0 m/s (i) 0.25% CNTs; v = 2.0 m/s

Fig. 15 Response of composite sensors with different contents of CNTs to impact loading

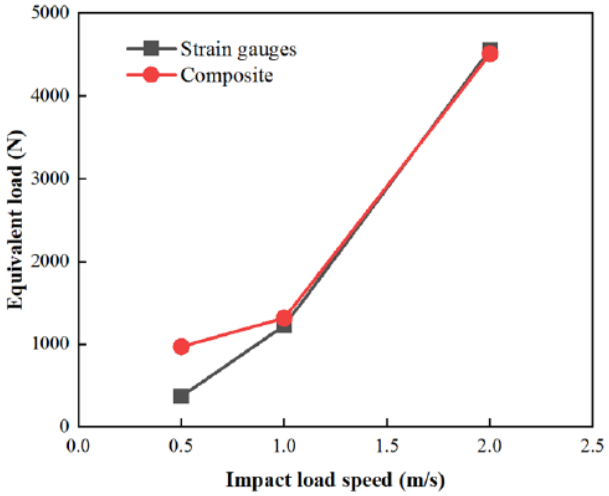

Fig. 16 Equivalent load comparison between strain gauges and composite

of a structure during construction or embedded into existing structures (Sasmal *et al*. 2017). This installation method offers protection against environmental erosion, ensuring the sensor's sensitivity and enabling accurate collision signal detection during ship-bridge collisions. Consequently, the application of this sensor for ship-bridge collision monitoring is highly feasible.

Fig. 16 shows the comparison of equivalent loads of strain gauges and composites. It can be seen that the equivalent load of the composite material is larger when the impact load velocity is small. The equivalent load of the composites maintains good correspondence with the measured values of strain gauges at impact load velocities of 1 m/s and 2 m/s, which indicates that CNT cementitious composites are more feasible to be used for ship-bridge collisions monitoring.

5. Conclusions

A novel sensor model for CNT cementitious composites, considering pore conductivity, was proposed for monitoring ship-bridge collisions in complex marine environments. The electrical response of the sensor was thoroughly analyzed, and the model's feasibility was verified through uniaxial compression tests and impact loading tests on cementitious composites with varying CNT contents. The primary

conclusions drawn from this study are as follows:

- CNT channels and pore solution channels were identified as significant conduction pathways for electrical conductivity in the composite material. The new model established takes into account the influence of pore conductivity on the electrical properties of the composites. This improved model has a higher accuracy compared to the model that ignores pore conductivity, and the calculated and experimental values for both types of models remain below 8% error in both axial and lateral directions, providing a valuable approach to sensor parameter design.
- The increase in the aspect ratio improves the sensitivity of the sensor. At a model aspect ratio of 1:4, a significantly higher rate of change of resistance is exhibited under axial loading. This variation can reach a maximum of 281% in the 10kN load range for transverse loading. These findings offer valuable insights for sensor design and engineering applications.
- The electrical response of CNT cementitious composites following impact loading demonstrated a consistent and distinctive pattern. In particular, a strong correlation was maintained between the electrical response of the sensor and the measured values of the strain gauge after impact loading when the impact load was between 1 m/s and 2 m/s. These results provide a theoretical basis for utilizing the sensor for ship-bridge collision monitoring.

Acknowledgments

Funding: This work was supported by the National Key R&D Program of China (Grant Number. 2024YFC3015200), the Key Program of Natural Science Foundation of Sichuan Province of China (Grant Number. 2025ZNSFSC0028), and National Natural Science Foundation of China (Grant Numbers. U1709207, 52078461).

Declaration of interest statement

The authors declare that they have no competing financial interests or personal relationships that could have appeared to influence the work reported.

Data availability statements

The data used in the current study are available from the corresponding author on reasonable request.

References

Cao, J. and Chung, D.D.L. (2004), "Electric polarization and depolarization in cement-based materials, studied by apparent electrical resistance measurement", *Cem. Concrete Res.*, **34**(3), 481-485. https://doi.org/10.1016/j.cemconres.2003.09.003

Christensen, R.M. and Lo, K. (1979), "Solutions for effective shear properties in three phase sphere and cylinder models", *J. Mech. Phys. Solids*, **27**(4), 315-330. https://doi.org/10.1016/0022-5096(79)90032-2

Danoglidis, P.A., Konsta-Gdoutos, M.S., Gdoutos, E.E. and Shah, S.P. (2016), "Strength, energy absorption capability and self-sensing properties of multifunctional carbon nanotube reinforced mortars", *Constr. Build. Mater.*, **120**, 265-274. https://doi.org/10.1016/j.conbuildmat.2016.05.049

Deng, F. and Zheng, Q.S. (2008), "An analytical model of effective electrical conductivity of carbon nanotube composites", *Appl. Phys. Lett.*, **92**(7). https://doi.org/10.1063/1.2857468

Duan, H.L., Jiao, Y., Yi, X., Huang, Z.P. and Wang, J. (2006), "Solutions of inhomogeneity problems with graded shells and application to core–shell nanoparticles and composites", *J. Mech. Phys. Solids*, **54**(7), 1401-1425. https://doi.org/10.1016/j.jmps.2006.01.005

Fantuzzi, N., Tornabene, F., Bacciocchi, M. and Dimitri, R. (2017), "Free vibration analysis of arbitrarily shaped Functionally Graded Carbon Nanotube-reinforced plates", *Compos. Part B: Eng.*, **115**, 384-408. https://doi.org/10.1016/j.compositesb.2016.09.021

García-Macías, E., D'Alessandro, A., Castro-Triguero, R., Perez-Mira, D. and Ubertini, F. (2017), "Micromechanics modeling of the uniaxial strain-sensing property of carbon nanotube cement-matrix composites for SHM applications", *Compos. Struct.*, **163**, 195-215. https://doi.org/10.1016/j.compstruct.2016.12.014

Han, B., Yu, X., Kwon, E. and Ou, J. (2012), "Effects of CNT concentration level and water/cement ratio on the piezoresistivity of CNT/cement composites", *J. Compos. Mater.*, **46**(1), 19-25. https://doi.org/10.1177/0021998311401114

Iijima, S. (1991), "Helical microtubules of graphitic carbon", *Nature*, **354**(6348), 56-58. https://doi.org/10.1038/354056a0

Khater, H.M. and Abd el Gawaad, H.A. (2015), "Characterization of alkali activated geopolymer mortar doped with MWCNT", *Adv. Mater. Res., Int. J.*, **4**(1), 045. https://doi.org/10.12989/amr.2015.4.1.045

Kim, H.K., Park, I.S. and Lee, H.K. (2014), "Improved piezoresistive sensitivity and stability of CNT/cement mortar composites with low water–binder ratio", *Compos. Struct.*, **116**, 713-719. https://doi.org/10.1016/j.compstruct.2014.06.007

Kim, G.M., Park, S.M., Ryu, G.U. and Lee, H.K. (2017), "Electrical characteristics of hierarchical conductive pathways in cementitious composites incorporating CNT and carbon fiber", *Cem. Concrete Compos.*, **82**, 165-175. https://doi.org/10.1016/j.cemconcomp.2017.06.004

Konsta-Gdoutos, M.S., Metaxa, Z.S. and Shah, S.P. (2010), "Highly dispersed carbon nanotube reinforced cement based materials", *Cem. Concrete Res.*, **40**(7), 1052-1059. https://doi.org/10.1016/j.cemconres.2010.02.015

Konsta-Gdoutos, M.S. and Aza, C.A. (2014), "Self sensing carbon nanotube (CNT) and nanofiber (CNF) cementitious composites for real time damage assessment in smart structures", *Cem. Concrete Compos.*, **53**, 162-169. https://doi.org/10.1016/j.cemconcomp.2014.07.003

Kumar, S., Kolay, P., Malla, S. and Mishra, S. (2012), "Effect of multiwalled carbon nanotubes on mechanical strength of cement paste", *J. Mater. Civ. Eng.*, **24**(1), 84-91. https://doi.org/10.1061/(ASCE)MT.1943-5533.0000350

Lee, H.K., Jang, D., Yoon, H.N., Yang, B., Seo, J. and Farooq, S.Z. (2022), "Synergistic effects of CNT and CB inclusion on the piezoresistive sensing behaviors of cementitious composites blended with fly ash", *Smart Struct. Syst., Int. J.*, **29**(2), 351-359. https://doi.org/10.12989/sss.2022.29.2.351

Li, G.Y., Wang, P.M. and Zhao, X. (2007), "Pressure-sensitive

properties and microstructure of carbon nanotube reinforced cement composites", *Cem. Concrete Compos.*, **29**(5), 377-382. https://doi.org/10.1016/j.cemconcomp.2006.12.011

Meira, G.R., Andrade, C., Alonso, C., Borba Jr, J.C. and Padilha Jr, M. (2010), "Durability of concrete structures in marine atmosphere zones–The use of chloride deposition rate on the wet candle as an environmental indicator", *Cem. Concrete Compos.*, **32**(6), 427-435. https://doi.org/10.1016/j.cemconcomp.2010.03.002

Mohammadimehr, M. and Alimirzaei, S. (2017), "Buckling and free vibration analysis of tapered FG-CNTRC micro Reddy beam under longitudinal magnetic field using FEM", *Smart Struct. Syst., Int. J.*, **19**(3), 309-322. https://doi.org/10.12989/sss.2017.19.3.309

Mori, T. and Tanaka, K. (1973), "Average stress in matrix and average elastic energy of materials with misfitting inclusions", *Acta. Metall.*, **21**(5), 571-574. https://doi.org/10.1016/0001-6160(73)90064-3

Park, J., Sung, Y.H., On, S.Y., Kwon, O.H., Bang, H., Kim, S.S., Han, J.H. and Lee, J.R. (2021), "Development of wireless SHM sensor node for in-flight real-time monitoring using embedded CNT fiber sensors", *Smart Struct. Syst., Int. J.*, **28**(3), 333-341. https://doi.org/10.12989/sss.2021.28.3.333

Parvaneh, V. and Khiabani, S.H. (2019), "Mechanical and piezoresistive properties of self-sensing smart concretes reinforced by carbon nanotubes", *Mech. Adv. Mater. Struct.*, **26**(11), 993-1000. https://doi.org/10.1080/15376494.2018.1432789

Rostami, R., Rahaghi, M.I. and Mohammadimehr, M. (2020), "Nonlinear forced vibration of sandwich plate with considering FG core and CNTs reinforced nano-composite face sheets", *Smart Struct. Syst., Int. J.*, **26**(2), 185-193. https://doi.org/10.12989/sss.2020.26.2.185

Saafi, M. (2009), "Wireless and embedded carbon nanotube networks for damage detection in concrete structures", *Nanotechnology*, **20**(39), p. 395502. https://doi.org/10.1088/0957-4484/20/39/395502

Sahoo, N.G., Rana, S., Cho, J.W., Li, L. and Chan, S.H. (2010), "Polymer nanocomposites based on functionalized carbon nanotubes", *Prog. Polym. Sci.*, **35**(7), 837-867. https://doi.org/10.1016/j.progpolymsci.2010.03.002

Sasmal, S., Ravivarman, N., Sindu, B.S. and Vignesh, K. (2017), "Electrical conductivity and piezo-resistive characteristics of CNT and CNF incorporated cementitious nanocomposites under static and dynamic loading", *Compos. Part A: Appl. Sci. Manuf.*, **100**, 227-243. https://doi.org/10.1016/j.compositesa.2017.05.018

Simmons, J.G. and Unterkofler, G.J. (1963), "Potential barrier shape determination in tunnel junctions", *J. Appl. Phys.*, **34**(6), 1828-1830. https://doi.org/10.1063/1.1702693

Suchorzewski, J., Prieto, M. and Mueller, U. (2020), "An experimental study of self-sensing concrete enhanced with multi-wall carbon nanotubes in wedge splitting test and DIC", *Constr. Build. Mater.*, **262**, p. 120871. https://doi.org/10.1016/j.conbuildmat.2020.120871

Takeda, T., Shindo, Y., Kuronuma, Y. and Narita, F. (2011), "Modeling and characterization of the electrical conductivity of carbon nanotube-based polymer composites", *Polymer*, **52**(17), 3852-3856. https://doi.org/10.1016/j.polymer.2011.06.046

Theodosiou, T.C. and Saravanos, D.A. (2010), "Numerical investigation of mechanisms affecting the piezoresistive properties of CNT-doped polymers using multi-scale models", *Compos. Sci. Technol.*, **70**(9), 1312-1320. https://doi.org/10.1016/j.compscitech.2010.04.003

Ubertini, F., Materazzi, A.L., D'Alessandro, A. and Laflamme, S. (2014), "Natural frequencies identification of a reinforced concrete beam using carbon nanotube cement-based sensors", *Eng. Struct.*, **60**, 265-275. https://doi.org/10.1016/j.engstruct.2013.12.036

Wen, S. and Chung, D.D.L. (2001), "Effect of carbon fiber grade on the electrical behavior of carbon fiber reinforced cement", *Carbon*, **39**(3), 369-373. https://doi.org/10.1016/S0008-6223(00)00127-5

Xie, X.L., Mai, Y.W. and Zhou, X.P. (2005), "Dispersion and alignment of carbon nanotubes in polymer matrix: a review", *Mat. Sci. Eng. R*, **49**(4), 89-112. https://doi.org/10.1016/j.mser.2005.04.002

Xu, J., Zhong, W. and Yao, W. (2010), "Modeling of conductivity in carbon fiber-reinforced cement-based composite", *J. Mater. Sci.*, **45**, 3538-3546. https://doi.org/10.1007/s10853-010-4396-5

Yasuoka, T., Shimamura, Y. and Todoroki, A. (2010), "Electrical resistance change under strain of CNF/flexible-epoxy composite", *Adv. Compos. Mater.*, **19**(2), 123-138. https://doi.org/10.1163/092430410X490446

Zhang, X.X., Meng, Q.J., Wang, X.C. and Bai, S.H. (2011), "Poly (adipic acid-hexamethylene diamine)-functionalized multi-walled carbon nanotube nanocomposites", *J. Mater. Sci.*, **46**, 923-930. https://doi.org/10.1007/s10853-010-4836-2

Zidour, M., Zerrouki, R., Hamidi, A., Tlidji, Y., Karas, A. and Tounsi, A. (2022), "Free vibration responses of nonlinear FG-CNT distribution in a polymer matrix", *Smart Struct. Syst., Int. J.*, **30**(2), 135-143. https://doi.org/10.12989/sss.2022.30.2.135

FC